Nontensorial Anisotropy of the Optical Field Effect at Thresholds and Saddle-Point Edges*

J. C. PHILLIPS†
Department of Physics and Institute of Metals, University of Chicago, Chicago, Illinois
(Received 17 January 1966; revised manuscript received 22 February 1966)

Previous treatments of the optical field effect at direct interband threshold (Franz-Keldysh effect) are generalized to saddle-point edges (Seraphin effect). The discussion demonstrates that nontensorial anisotropies are present in both cases. For practical reasons, however, it appears that nontensorial anisotropy should be easier to observe in the Seraphin effect than in the Franz-Keldysh effect. The anisotropy enables one to assign an edge to interband critical points located in specific regions in the Brillouin zone, and thus provides a powerful tool for solid-state spectroscopy. Strain and nonlinear effects are discussed briefly.

1. INTRODUCTION

WHEN a static electric field is applied to an insulator, optical absorption in the vicinity of an interband threshold is altered. The theory of this effect was first discussed by Franz[1] and by Keldysh[2] who found that it produced an exponential tail below the zero-field threshold, as well as oscillations above threshold. The width of the tail, as well as the period of oscillations, is of order

$$\Delta E \approx (eFa)^{2/3}(E_{BZ})^{1/3}. \tag{1.1}$$

In (1.1) the electric field is F, the lattice constant is a, and $E_{BZ}=\hbar^2/ma^2\approx 10$ eV is roughly the kinetic energy of a Wannier wave packet. The Franz-Keldysh terms are different from the Stark splittings[3]

$$\delta E \approx eFa, \tag{1.2}$$

of the Wannier states. In practice $\Delta E \gtrsim 10\delta E$, so that the Franz-Keldysh effect is observable in many crystals at fields below the breakdown field, while the Stark splittings have so far not been resolved. Thus the Franz-Keldysh effect is truly crystalline in character, in contrast to the Stark splittings (1.2) which arise from Wannier levels.[3]

The Stark effect is useful as a diagnostic tool in identifying atomic transitions. Similarly we expect the Franz-Keldysh effect to be useful in identifying interband edges in the fundamental absorption spectra of insulators. This has recently been shown to be the case in beautiful experiments by Seraphin and co-workers.[4] They have demonstrated that in Ge modulated electroreflectance is capable of identifying edges in the fundamental absorption spectrum with a resolution of at least 0.003 eV, which is not much less accurate than the resolution achieved at threshold of 0.001 eV. Another geometry for electro-reflectance has been developed by Shaklee, Pollak and Cardona[5] which appears to be even simpler and more flexible.

The utility of electro-reflectance experiments in the fundamental absorption region stems, as we have previously noted,[6] from the fact that at saddle-point edges in the imaginary part ϵ_2 of the dielectric response an effect is found which is complementary to the Franz-Keldysh effect at thresholds in ϵ_2. This duality theorem, which is illustrated in Fig. 1, has been confirmed experimentally.[7]

The purpose of this note is to explore in qualitative fashion the polarization dependence of the electroreflectance signals, especially near saddle-point edges. In doing so we borrow liberally from previous treatments of the Franz-Keldysh effect, and transcribe only those equations essential to our qualitative analysis.

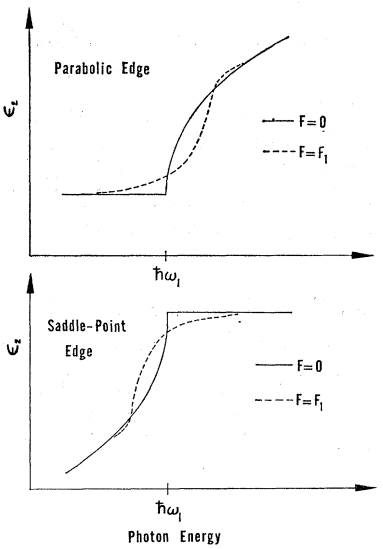

FIG. 1. A sketch depicting the change in ϵ_2 at a threshold or a saddle-point edge (applied field F parallel to the principal axis of the saddle point). The sketch illustrates the duality theorem discussed in the text.

* Supported in part by Office of Naval Research and a general grant to Institute for the Study of Metals by Advanced Research Projects Agency.

† Alfred P. Sloan Fellow.

[1] W. Franz, Z. Naturforsch. **13a**, 484 (1958).

[2] W. L. Keldysh, Zh. Eksperim. i Teor. Fiz. **34**, 1138 (1958) [English transl.: Soviet Phys.—JETP **7**, 788 (1958)].

[3] J. Callaway, Phys. Rev. **130**, 549 (1963); **134**, A998 (1964); K. Tharmalingam, *ibid.* **130**, 2204 (1963).

[4] B. O. Seraphin and R. B. Hess, Phys. Rev. Letters **14**, 138 (1965).

[5] K. L. Shaklee, F. H. Pollak, and M. Cardona, Phys. Rev. Letters **15**, 883 (1965).

[6] J. C. Phillips and B. O. Seraphin, Phys. Rev. Letters **15**, 107 (1965). J. C. Phillips, Varenna Lectures, Italian Physical Society (to be published).

[7] B. O. Seraphin, Phys. Rev. **140**, A1716 (1965).

2. PHASE-SPACE INTEGRALS

Near an interband critical point $\mathbf{k}_c$ defined by

$$\nabla_{\mathbf{k}}[E_c(\mathbf{k})-E_v(\mathbf{k})]_{\mathbf{k}=\mathbf{k}_c}\equiv[\nabla_{\mathbf{k}}E_{cv}(\mathbf{k})]_{\mathbf{k}=\mathbf{k}_c}=0, \quad (2.1)$$

we may expand $E_{cv}(\mathbf{k})$ to second order in $\mathbf{k}-\mathbf{k}_c$. For convenience we set $\mathbf{k}_c$ equal to zero and assume that the valence and conduction bands are nondegenerate at $\mathbf{k}_c$. Then choosing principal axes suitably we have

$$E_{cv}(\mathbf{k})=E_g+\tfrac{1}{2}\hbar^2\textstyle\sum_i k_i^2/\mu_i, \quad (2.2)$$

$$E_g=E_{cv}(0)=\hbar\omega_1. \quad (2.3)$$

For an arbitrary orientation of the static field $\mathbf{F}$ we may write

$$\mathbf{F}=\textstyle\sum_i F_i\hat{e}_i, \quad (2.4)$$

where $\hat{e}_i$ denote unit vectors along the principal axes of (2.2) and

$$F_i=F\cos\theta_i. \quad (2.5)$$

We now put $F_i=F\delta_{ij}$ and separate phase-space sums into longitudinal and transverse components. Apart from constant factors the imaginary part of the dielectric function ϵ_2 is given by

$$\epsilon_2\propto\sum_{\mathbf{k}_c,\mathbf{k}_v}|M_{cv}|^2\delta(E_c-E_v-\hbar\omega)\delta(\mathbf{k}_c-\mathbf{k}_v), \quad (2.6)$$

where the matrix element M_{cv} can be written as

$$M_{cv}\propto\Phi(0), \quad (2.7a)$$

$$M_{cv}\propto|\nabla_r\Phi(0)|, \quad (2.7b)$$

according as the edge in question is dipole Eq. (2.7a) allowed or Eq. (2.7b) forbidden.[3] The wave function $\Phi(r)$ is the envelope function giving the amplitude of the Bloch states $\psi_c(\mathbf{r}_e)\psi_v(\mathbf{r}_h)$ as a function of $\mathbf{r}=\mathbf{r}_e-\mathbf{r}_h$. Henceforth we restrict ourselves to case Eq. (2.7a).

In the presence of the electric field F_j it is convenient to define

$$\tau=E-E_g-\tfrac{1}{2}\hbar^2(k_l^2/\mu_l+k_m^2/\mu_m), \quad (2.8)$$

$$\theta_F^3=e^2F^2/2\hbar\mu_j, \quad (2.9)$$

where θ_F if real, as well as the Airy function

$$\mathrm{Ai}(\beta)=\frac{1}{\sqrt{\pi}}\int_0^\infty\cos(\tfrac{1}{3}u^3+\beta u)du. \quad (2.10)$$

Apart from constant factors we then have[3]

$$\Phi(0)\propto(F^{1/2}/\theta_F)\,\mathrm{Ai}(-\tau/\hbar\theta_F). \quad (2.11)$$

The Airy function is an integral function whose asymptotic expansions for $|\beta|\to\infty$ are

$$\mathrm{Ai}(\beta)\propto\beta^{-1/4}\exp(-2\beta^{3/2}/3), \quad (2.12a)$$

$$\mathrm{Ai}(-\beta)\propto\beta^{-1/4}\sin(\tfrac{2}{3}\beta^{3/2}+\pi/4). \quad (2.12b)$$

When (2.7a) and (2.11) are substituted in (2.6), one obtains for ω near ω_1 a contribution to ϵ_2 of the form

$$\epsilon_{2c}\propto\frac{F}{\theta_F^2}\int\int_0^{K_{\max}}dk_l dk_m\left|\mathrm{Ai}\left(\frac{-\tau}{\hbar\theta_F}\right)\right|^2, \quad (2.13)$$

where $K_{\max}$ is a fraction of a Brillouin-zone radius which we may allow to tend to ∞.

We now assume that both μ_l and μ_m are positive. If μ_j is positive also, we have the Franz-Keldysh case of interband thresholds, with $\theta_F>0$. Then if $\omega<\omega_1$ from (2.8) we see that $\tau<0$ and from (2.12a) one obtains an exponential tail. Introducing new variables

$$t_l^2=(\hbar k_l)^2/2\mu_l\theta_F, \quad t_m^2=(\hbar k_m)^2/2\mu_m\theta_F \quad (2.14)$$

we find that with $s=t_l^2+t_m^2$

$$\epsilon_{2c}\propto\mu^{3/2}\theta_F^{1/2}\int_{(\omega_1-\omega)/\theta_F}^\infty 2\pi ds\,|\mathrm{Ai}(s)|^2 \quad (2.15)$$

$$\mu^3=\mu_j\mu_l\mu_m. \quad (2.16)$$

For $\omega<\omega_1$ the explicit result is

$$\epsilon_{2c}\propto(\mu_l\mu_m)^{1/2}(F/(\omega-\omega_1))\times\exp[-\tfrac{4}{3}((\omega_1-\omega/\theta_F))^{3/2}] \quad (2.17)$$

which is not valid if ω is too close to ω_1. From (2.17) we see that the strength of the linear tail is proportional to $\mu_1=(\mu_l\mu_m)^{1/2}$.

The asymptotic expressions (2.12) are not convenient for $\omega-\omega_1\approx 0$. Seraphin and Bottka[8] have evaluated (2.15) with $\mu\simeq 0.07$ for a range of field strengths appropriate to laboratory conditions, $F\approx 10^5$ volts/cm. The results for $\Delta\epsilon_{2c}$, the field-induced change in ϵ_{2c}, are shown for a parabolic edge in Fig. 2, which exhibits

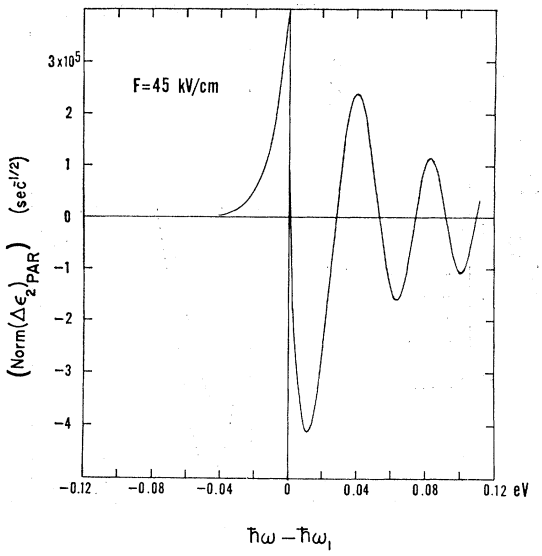

FIG. 2. The change $\Delta\epsilon_2$ induced by an applied field at a parabolic threshold (after Ref. 8). Exciton and lifetime effects are neglected.

[8] B. O. Seraphin and N. Bottka, Phys. Rev. 139, A560 (1965).

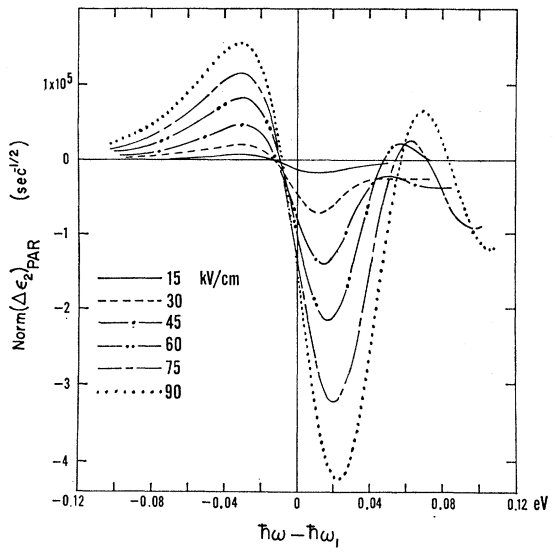

FIG. 3. The effect of lifetime broadening (Lorentzian convolution with $\gamma=0.035$ eV) on the values of $\Delta\epsilon_2$ shown in Fig. 2 (after Ref. 8).

the exponential tail for $\omega<\omega_1$ and damped oscillations for $\omega>\omega_1$. When the effects of lifetime broadening are included, the first dip for $\omega>\omega_1$ gives the largest effect, as shown in Fig. 3. The narrow peak at $\omega=\omega_1$ is washed out, and both the exponential tail and the second oscillation appear as satellites to the main dip.

The oscillations for $\omega>\omega_1$ arise as follows: According to (2.8) in this case there is an elliptical region centered on $k_l=k_m=0$ for which $\tau\geq 0$ and $\mathrm{Ai}(-\tau/\hbar\theta_F)$ oscillates as indicated by the asymptotic expansion (2.12b). Even using (2.12b) for all $\tau\geq 0$ leads to sums over k_l and k_m which cannot be evaluated in closed form, and when these are treated approximately the magnitude of the first dip is found[3] to be independent of F, which is not the case according to Fig. 2. When the effects of lifetime broadening are included, as shown in Fig. 3, the dependence of the magnitude of the dip on F is greater still.

The period of the oscillations can be obtained roughly from (2.12b). It is given by[3]

$$\Delta(\omega)=\pi(2\hbar)^{-1/2}(F\mu_j/\mu_1^{3/2})(\omega-\omega_1)^{-1/2}. \quad (2.18)$$

Through the factor $\mu_j/\mu_1^{3/2}$ this period is strongly anisotropic; this anisotropy might be used to identify the symmetry of an interband threshold.

Now suppose that one of the three μ_i is negative while the other two are positive (M_1-type saddle-point edges). If μ_j is negative (F parallel to the principal axis of the saddle point), then τ is unchanged, but θ_F reverses sign compared to the threshold case. This causes the exponential tail in $\Delta\epsilon_2$ which is found below threshold $\omega<\omega_1$ to shift above the saddle-point edge $\omega>\omega_1'$. Also the oscillations in $\Delta\epsilon_2$ which are found above threshold, $\omega>\omega_1$, lie below the saddle-point edge $\omega<\omega_1'$. Finally, the sign of $\Delta\epsilon_2$ near the saddle-point edge ω_1' is reversed compared to its contribution near the threshold edge ω_1.

These results are summarized by the duality theorem (indicated in Fig. 1): To obtain the effect of an electric field on a saddle-point edge when the field is parallel to the principal axis of the edge, replace $(\omega-\omega_1)$ by $(\omega_1'-\omega)$, and replace $\Delta\epsilon_2$ by $-\Delta\epsilon_2$. This theorem may be verified in detail by repeating each step of the calculations given, e.g., by Callaway.[3]

How are these results changed when F is not parallel to the principal axis of the saddle point? According to (2.4) we must analyze the case μ_j, $\mu_l>0$, i.e., F_j is perpendicular to the principal axis m of the saddle point. According to (2.8) the transverse variable τ no longer has a threshold at $\omega=\omega_1$, associated with which there is a step function $\theta(\omega-\omega_i')$ in the transverse, two-dimensional density of states. Instead we have a two-dimensional saddle-point, which gives rise to a weaker logarithmic singularity in the transverse density of states.

We have seen that the largest effect for both parabolic edges and saddle-point edges (longitudinal orientation on F) is the first dip which modulates the square-root edge $[(\omega-\omega_1)^{1/2}$ or $-(\omega_1'-\omega)^{1/2}$, respectively]. This dip is associated with the closed region centered on $k_l=k_m=0$ for which $\tau>0$. In the transverse orientation $F_i=F\delta_{im}$ the region is no longer closed. To treat this case introduce

$$\gamma_F{}^3=e^2F^2/2\hbar\mu_m \quad (2.19)$$

as well as the parabolic coordinates

$$u=\hbar k_j{}^2/2\mu_j-\hbar k_l{}^2/2\mu_l$$
$$v=\hbar k_jk_l/2(\mu_j\mu_l)^{1/2}.$$

Including the Jacobean for the new coordinates the phase-space sum analogous to (2.13) becomes

$$\epsilon_{2c}\alpha\frac{F}{\gamma_F{}^2}\int\int_S\frac{dudv}{2(u^2+v^2)^{1/2}}|\mathrm{Ai}[(\delta\omega-u)/\gamma_F]|^2, \quad (2.20)$$

where $\delta\omega=\omega-\omega_1'$ and S is the open region making the dominant contribution to (2.20). This is just the region bordering the lines

$$u=0=k_j\mu_l{}^{1/2}\pm k_l\mu_j{}^{1/2}. \quad (2.21)$$

Denote the frequency difference between ω_1' and the nearest edge at ω_2 by the cutoff frequency

$$\omega_c=|\omega_1'-\omega_2|. \quad (2.22)$$

Also introduce the parameter Γ as several times the lifetime broadening or the period of the Airy function. Then we can make a strip approximation to S and (2.20) becomes

$$\epsilon_{2c}\propto\frac{F}{\gamma_F{}^2}\int_{\delta\omega-\Gamma}^{\delta\omega+\Gamma}du\left|\mathrm{Ai}\left[\frac{\delta\omega-u}{\gamma_F}\right]\right|^2\int_{-\omega_c}^{\omega_c}\frac{dv}{2(u^2+v^2)^{1/2}}$$
$$\propto\mu^{3/2}\gamma_F{}^{1/2}\int_{(\delta\omega-\Gamma)/\gamma_F}^{(\delta\omega+\Gamma)/\gamma_F}du\ln\left(\frac{2\omega_c}{u}\right)|\mathrm{Ai}(\delta\omega-u)|^2, \quad (2.23)$$

where we have assumed that $\omega_c\gg\Gamma$.

Comparing (2.23) with (2.15) we note two differences. In place of the constant factor 2π in (2.15) arising from the angular integration the integrand of (2.23) contains the amplification factor

$$A(u)=\ln(2\omega_c/u). \tag{2.24}$$

We may estimate the magnitude of A if ω_c and the period Δ of the oscillations are known; then $A\approx(2\omega_c/\Delta)$.

The second difference has to do with the replacement of θ_F in (2.15) by γ_F in (2.23). The effect of this change is difficult to estimate. To the extent that the strength of the dip is linear in F we may infer from (2.17) that (2.15) is multiplied by $\mu_j^{-1/2}$ while (2.23) is multiplied by $\mu_m^{-1/2}$. According to Fig. 3 this may not be a poor approximation for some edges.

3 RELATION TO EXPERIMENT

According to the results of the preceding section, the dynamic contribution to the Seraphin field effect on a saddle-point edge of type M_1 (two principal components of $\mu>0$, the third, along the j axis, <0), is a sensitive function of the orientation of the applied field **F**. Omitting the tensorially dependent oscillator strengths we found that

(a) For **F** parallel to the j axis, the effect is conjugate to the Franz-Keldysh effect as illustrated by Fig. 1, and

(b) For **F** perpendicular to the j axis, the effect is similar to the Franz-Keldysh effect, but the integrand contains an amplification factor, roughly of order $A/2\pi=\ln(2\omega_c/\Delta)/2\pi$. With $\hbar\omega_c\approx0.5$ eV, and $\Delta\approx0.05$ eV, we have $A/2\pi\approx0.5$.

Oscillator strengths in general will modify these conclusions as follows: In case (a) the region determining the dip is closed and centered on the critical point. It is easy to see that to lowest order in $\delta\mathbf{k}^2=(\mathbf{k}-\mathbf{k}_c)^2$ we may use the oscillator strengths of the bands at $\mathbf{k}_c$. In case (b) the situation is more complex. The appearance of the upper cutoff ω_c in the amplification factor A suggests that the **k** dependence of the oscillator strengths as well as terms of order quartic and higher in k_j and k_l will affect the value of ω_c that should be used in (2.24). For qualitative purposes it may be sufficient to change ω_c slightly; because of the logarithmic dependence of A on ω_c this factor may not be greatly altered. To proceed further, we must choose a specific band model.

The model we consider places the critical points associated with the interband edges along equivalent cylindrically symmetric axes of the Brillouin zone. To be specific we assume that the crystal has cubic symmetry, so that the equivalent axes could be $\Delta=\langle1,0,0\rangle$, or $\Lambda=\langle1,1,1\rangle$. Then consider first a case of common occurrence in semiconductors, that the initial states are the two-fold degenerate states Δ_5, which have (p_y,p_z) symmetry, or Λ_3, which have $(p_x-p_y, p_x+p_y-2p_z)$ symmetry. The final states are Δ_1 or Λ_1 (s symmetry).

After summing over equivalent valleys the oscillator strength transforms in general as a second-rank tensor. In the case considered here we assume that unpolarized light is reflected at normal incidence, so that the radiation field **E** is transverse to the dc field **F**. Then the oscillator strength f_i of the ith valley with principal axis along the ith symmetry axis is

$$f_i\propto 1+\cos^2\theta_i, \tag{3.1}$$

where θ_i is the angle that **F** makes with the principal axis j of the ith valley. We assume that at each angle we can superpose the linear effects associated with the longitudinal and transverse components of **F**. (This is not strictly correct, but it represents a simple interpolation formula for $0<\theta<\pi/2$.) According to (a) and (b) above, ϵ_{2c} is positive for $\omega<\omega_1'$ and negative for $\omega>\omega_1'$ for both components. The largest contribution of the longitudinal component, however, occurs as a peak for $\omega<\omega_1'$, while the transverse components give an effect similar to the parabolic edge and make their largest contribution as a dip for $\omega>\omega_1'$. (See Fig. 3.) In each case the peak/dip is about 3 times greater than the dip/peak at higher/lower frequency, respectively.

The separate contributions to ϵ_{2c} may be estimated if we know ω_c, Δ, the longitudinal mass μ_j, and the transverse mass $\mu_m=\mu_t$. The peak and dip dynamical contributions D_i of each critical point have the explicit forms

	$\omega<\omega_1'$	$\omega>\omega_1'$
long.	$3\lvert\cos\theta_i\rvert\mu_j^{-1/2}$	$-\lvert\cos\theta_i\rvert\mu_j^{-1/2}$
trans.	$\lvert\sin\theta_i\rvert\mu_t^{-1/2}A/2\pi$	$-3\lvert\sin\theta_i\rvert\mu_t^{-1/2}A/2\pi$

(3.2)

In arriving at (3.2) we have made a number of simplifying approximations. Some of these are not essential, and could be removed by more accurate computation of the phase-space sums over the Airy functions.[9] Some of the approximations, however, are inherent because of lifetime broadening and uncertainties in the band structure as regards the effective mass components, nonparabolic kinetic energies, and **k**-dependent oscillator strengths.

Now let us consider the $\Lambda_3\rightarrow\Lambda_1$ edge in Ge studied by Seraphin. Here $(\mu_j/\mu_t)^{1/2}\approx5$ and $A/2\pi\approx0.5$. Combining (3.1) and (3.2) to obtain the intensity $I_i=f_iD_i$ of each critical points' contribution to the total change $\Delta\epsilon_2$ at the edge we have

$$\Delta\epsilon_2=\textstyle\sum_i f_iD_i. \tag{3.3}$$

From (3.3) the change in an observable such as the reflectivity R is obtained as

$$\Delta R=\alpha\Delta\epsilon_1+\beta\Delta\epsilon_2, \tag{3.4}$$

where α and β are known functions of ϵ_1 and ϵ_2, and $\Delta\epsilon_1$ is obtained from $\Delta\epsilon_2$ using the Kramers-Kronig relations. With $(\mu_j/\mu_t)^{1/2}=5$ and $A/2\pi=0.5$, the tableau (3.2) will have the greatest contribution (for most

[9] More quantitative evaluations of the integrals over Airy functions have been carried out by D. E. Aspnes (to be published).

TABLE I. Nontensorial anisotropy of the Seraphin effect at a direct interband saddle-point edge. The orientation of the static field F parallel to either ⟨1,1,1⟩, ⟨1,0,0⟩, or ⟨1,1,0⟩ crystalline axes is listed in the first row for the two cases I_σ and I_π. The location of the critical points k_c associated with the saddle-point edge along equivalent axes $\Delta=[1,0,0]$, or $\Lambda=[1,1,1]$ in the Brillouin zone is indicated in the first column.

	I_σ			I_π		
k_c/F	⟨1,0,0⟩	⟨1,1,1⟩	⟨1,1,0⟩	⟨1,0,0⟩	⟨1,1,1⟩	⟨1,1,0⟩
[1,1,1]	1.00	0.75	0.90	1.00	1.10	1.03
[1,0,0]	1.00	1.59	1.50	1.00	0.90	0.90

values of θ_i) in the lower right. Thus, we assume that the dominant structure in $\Delta\epsilon_2$ comes from the dip for $\omega>\omega_1'$ and estimate the relative magnitude of the dip from (3.3) as a function of the location $\mathbf{k}_c$ of the critical point and the orientation $\mathbf{F}$ of the applied field relative to the crystalline axes:

$$\Delta\epsilon_2 \propto \sum_i (1+\cos^2\theta_i)[|\cos\theta_i|+7.5|\sin\theta_i|]. \quad (3.5)$$

We have evaluated (3.5) assuming four equivalent edges along ⟨1,1,1⟩ axes or three equivalent edges along ⟨1,0,0⟩ axes, and normalized the results in each case to 1.00 for F along the ⟨1,0,0⟩ axes. The results are shown in Table I.

The first conclusion to be drawn from this table is that the summation on i in (3.5) considerably reduces the dependence of the effect on the orientation of $\mathbf{F}$ relative to the crystalline axes. Thus within the limits of the calculation the dependence of the $\Lambda_3 \rightarrow \Lambda_1$ edge on surface orientation would be difficult to observe, and little dependence was found for this edge in Ge.[10]

In Si between 3.3 and 3.5 eV three peaks have been observed in n-type samples[6] and only two in p-type samples.[8] The behavior of the middle dip in the n-type samples closely follows that of the highest peak, but the middle dip is absent in p-type samples. We therefore exclude the middle dip from the following discussion.

The two remaining structures, a dip at 3.33 eV and a peak at 3.41 eV, appear to be derived from parabolic and saddle-point edges, respectively. The intensity of the parabolic dip appears to be insensitive to the orientation of $\mathbf{F}$. It, therefore, provides a convenient calibration for the intensity of the saddle-point peak. Again normalizing to 1.0 for $\mathbf{F}$ along ⟨1,0,0⟩, the data give 2.0 and 1.6 for F along ⟨1,1,1⟩ and ⟨1,1,0⟩ axes. This agrees better with the second row of Table I (i.e., k_c along the $\Delta=[1,0,0]$ axes) than the first row (k_c along the $\Lambda=[1,1,1]$ axes).

This agreement with the Δ row is gratifying. Precise piezoreflectance experiments by Gerhardt[11] do indicate that the 3.4 eV edge has predominantly Δ symmetry. This edge is still not entirely understood, however. Appreciable temperature dependence of the edge is observed[12] at 100°K, i.e., at $\frac{1}{5}\theta$, where θ is the Debye temperature. Also the deformation potential parameters are unusually large.[11,13]

4 NONLINEAR EFFECTS

The field dependence of the magnitude of the central peak or dip appears to be strongly dependent on lifetime effects (see Fig. 3). Thus, while we expect to observe harmonics of the optical field effect, and while these should exhibit interesting anisotropies, their interpretation will be quite complicated. A much simpler nonlinear effect has been observed by Seraphin and Bottka at the fundamental frequency.[8] They vary the dc bias F_0 and fix the excursion δF of the field about F_0. They then find that as F_0 is increased the center of the oscillation shifts toward higher (lower) energies for parabolic (saddle-point edges), a result which is consistent with their calculations based on the duality theorem.

5. POLARIZATION EFFECTS

The examples discussed so far indicate the magnitude of effects to be expected in cubic crystals as the orientation of the static field $\mathbf{F}$ is varied relative to the crystal axes. It has been assumed that the propagation vector $\mathbf{q}$ of the light is parallel to $\mathbf{F}$ (which is the case in the geometries used at present[4,5]) and that the light is unpolarized.

If we retain the condition that $\mathbf{q}$ be parallel to $\mathbf{F}$, but use polarized light, then interesting effects can arise for $\mathbf{F}$ along $(1,1,0)=\Sigma$ axes. For example, in Si and Ge it is believed[14] that M_1 edges of Δ symmetry are quasi-degenerate with M_2 edges of Σ symmetry. The spin-orbit and heteropolar splittings of the M_1 edges have been observed in a number of III–V and II–VI compounds.[15] However, the M_2 edge has so far not been separated from the M_1 edge, nor has any M_2 edge been explicitly identified. Moreover, it has been suggested (see Fig. 55 of Ref. 15) that at low temperatures the M_1 and M_2 edges may be strongly distorted by exciton formation. In these circumstances polarization studies which can vary the intensity of the M_2 edge relative to the M_1 edge would be of great interest.

Let us now suppose that experiments can be done with $\mathbf{q}$ perpendicular to $\mathbf{F}$. Then the $\mathbf{E}$ radiation field may be either parallel (π) or perpendicular (σ) to $\mathbf{F}$. We may gain insight into the polarization effects expected by considering the $\Lambda_3 \rightarrow \Lambda_1$ or $\Delta_5 \rightarrow \Delta_1$ edges discussed in Sec. 3 for σ polarization. Now we find that the dynamical factors associated with $\mathbf{F}$ are unchanged,

[10] B. O. Seraphin (private communication).
[11] U. Gerhardt, Phys. Rev. Letters **15**, 401 (1965); Phys. Status Solidi **11**, 801 (1965).
[12] B. O. Seraphin and N. Bottka, Phys. Rev. Letters **15**, 104 (1965).
[13] I. Goroff and L. Kleinman, Phys. Rev. **132**, 1080 (1963).
[14] D. Brust, J. C. Phillips, and F. Bassani, Phys. Rev. Letters **9**, 94 (1962). D. Brust, M. L. Cohen, and J. C. Phillips, *ibid.* **9**, 389 (1962). D. Brust, Phys. Rev. **134**, A1337 (1964). M. L. Cohen and J. C. Phillips, *ibid.* **139**, A912 (1965).
[15] J. C. Phillips, *Solid State Physics*, edited by F. Seitz and D. Turnbull (Academic Press Inc., New York, 1966), Vol. 18, p. 56.

but that the oscillator strengths are

$$f_i(\pi)=1-\cos^2\theta_i. \tag{5.1}$$

When weighted by the dynamical factors (3.2) appropriate to a saddle point edge, both edges should show a dependence on polarization. The effects are of order 25–50% and can be studied for fixed orientation of $\mathbf{F}$, i.e., on the same sample. The polarization effects should, therefore, be easier to study than the orientation dependence.

6. CONCLUSIONS

Our purpose here has been to explore qualitatively the anisotropy of the Franz-Keldysh effect at a parabolic edge or the Seraphin effect at a saddle-point edge. Because of dynamical quantum-mechanical factors the anisotropy of both effects is nontensorial in character. However, the nontensorial character of the Franz-Keldysh effect is expected to be more difficult to demonstrate experimentally. The reason for this is that although nontensorial factors enter (2.17) and (2.18), these equations describe effects related to the magnitude of the satellites of the central dip, whose own magnitude is strongly influenced by lifetime effects. It is still possible that nontensorial behavior could be observed if thresholds not at $\mathbf{k}=0=\Gamma$ were studied. The Pb salts (PbTe, PbSe, PbS) appear to have direct thresholds at the equivalent {111} faces of the Brillouin zone.[16]

On the other hand, large nontensorial effects are expected at saddle-point edges in most cases. Apart from their intrinsic interest these anisotropies are expected to provide detailed information on the location $\mathbf{k}_c$ of interband edges in the fundamental absorption region comparable to the information provided by cyclotron resonance and magneto-optic experiments at band edges. Moreover it appears that the Seraphin effect gives information not only over a much broader energy range but also with much poorer samples.

In addition to the non-tensorial anisotropies discussed here for cubic crystals, stronger anisotropies can be achieved by studying crystals of lower symmetry. With cubic crystals greater anisotropy can be achieved by making the edges inequivalent and/or lifting the degeneracies by applying uniaxial strains. The combined strain and field effects should still exhibit nontensorial anisotropies different from the tensorial anisotropy expected from the symmetry of the strained crystal. Thus, the Seraphin effect is intrinsically richer for some purposes than piezo-optic differentials.

ACKNOWLEDGMENTS

In preparing this paper I have benefited from numerous discussions with B. O. Seraphin and U. Gerhardt. I wish to acknowledge especially stimulating correspondence from Dr. Gerhardt. I am grateful to Professor P. Handler for mentioning to me the extensive computations of D. E. Aspnes.

Note added in proof. Comparison of the results of Aspnes (Ref. 9) with Eqs. (2.20)–(2.23) of this paper shows several interesting differences. These arise because the integral (2.20) is divergent. We have obtained a convergent result by restricting attention to the strip S contained in one Brillouin zone. Aspnes' integrals diverge, but by utilizing the elegant device of subtracting the spectrum at $F=0$ from the spectrum with $F=F_0$, he obtains finite results for $\Delta\epsilon_2$ which exhibit the anisotropy in a form that is much more convenient than the one given here. Aspnes' results appear to provide an adequate basis for interpreting presently available spectra, which are taken with inhomogeneous applied fields. We believe, however, that the strip approximation may be better suited to high resolution studies of non-degenerate edges. I am grateful to Dr. Aspnes for correspondence on these points, and for providing a preprint of his paper prior to publication.

[16] P. J. Stiles, E. Burstein, and D. N. Logenburg, J. Appl. Phys. 32, 2174 (1961); J. B. Conklin, Jr., L. E. Johnson, and G. W. Pratt, Jr., Phys. Rev. 137, A1282 (1965).